Materials Today Chemistry 26 (2022) 101067

Contents lists available at ScienceDirect

Materials Today Chemistry

journal homepage: www.journals.elsevier.com/materials-today-chemistry/

Building large-scale unimolecular scaffolding for electronic devices

E. Escorihuela [a, b], A. Concellón [c], I. Marín [d], V.J. Kumar [e], L. Herrer [a, b, f], S.A. Moggach [e], A. Vezzoli [g], R.J. Nichols [g], P.J. Low [e], P. Cea [a, b, f], J.L. Serrano [a, d, **], S. Martín [a, b, f, *]

[a] Instituto de Nanociencia y Materiales de Aragón (INMA), CSIC-Universidad de Zaragoza, Zaragoza, 50009, Spain
[b] Departamento de Química Física, Facultad de Ciencias, Universidad de Zaragoza, 50009, Zaragoza, Spain
[c] Department of Chemistry, Massachusetts Institute of Technology, Cambridge, MA, 02139, USA
[d] Departamento de Química Orgánica, Facultad de Ciencias, Universidad de Zaragoza, 50009, Zaragoza, Spain
[e] School of Molecular Sciences, University of Western Australia, 35 Stirling Highway, Crawley, WA, 6009, Australia
[f] Laboratorio de Microscopias Avanzadas (LMA), Universidad de Zaragoza, Edificio I+D+i, 50018, Zaragoza, Spain
[g] Department of Chemistry, University of Liverpool, Liverpool, L69 7ZD, United Kingdom

ARTICLE INFO

Article history:
Received 5 May 2022
Received in revised form
16 June 2022
Accepted 27 June 2022
Available online xxx

Keywords:
Large area unimolecular devices
Layer-by-layer self-assembly
Metalloporphiryn
Wire-like oligophenylene

ABSTRACT

The fabrication of a future generation of (opto)electronic devices based on molecular components and materials will require careful chemical design, coupled with assembly methods that permit precise spatial orientation and arrangement of the functional molecules within device structures. Although unimolecular electronics are already a laboratory reality, the variation in the arrangement of the molecule within a molecular junction from measurement to measurement is considerable. Consequently, controlling the precise geometry at the molecule–metal contacts is a long-standing and largely unresolved challenge. Here, a strategy to fabricate uniform unimolecular junctions distributed in a regular pattern is reported. A monolayer of zinc metalloporphyrins, peripherally functionalised by bulky dendrons, is used to provide a well-defined array of molecular binding sites with precise spatial distribution. The dendrons are then photochemically cross-linked to form a robust base-layer. Parallel, uniformly-spaced unimolecular structures are subsequently assembled on these binding sites through a layer-by-layer (LbL) strategy. This LbL strategy proceeds through coordination of an α,ω-amino functionalised oligo(phenylene)ethynylene (OPE) molecule to the zinc ions of the metalloporphyrin template base-layer. The structure is then extended through alternating self-assembled layers of (cross-linked) zinc porphyrin and OPE. The coordination interaction between the zinc(II) sites and the bifunctional OPE wire ensures a high degree of registry between the layers and good electrical contact through the extended arrays and offer fine control over the chemical composition.

1. Introduction

Many properties of advanced materials rely on well-organized internal structures [1–3]. In this context, spatial orientation and control of the molecular arrangement of functional molecules in extended assemblies is of utmost importance in the fabrication of next-generation molecular electronic and optical devices [4]. Thus, whilst unimolecular electrode | molecule | electrode junctions are already a reality, with combinations of molecular design, electrode material and external gating all contributing to the fine-tuning of the electrical properties [5–9], variations in the individual response of each junction have so far largely impeded translation of single molecule electronics from the laboratory to device structures [10]. These inconsistencies arise from differences and fluctuations in the molecular conformation, the electrode–anchor contact geometry, or the electrode surface geometry within each junction [6,11,12]. Since molecular geometry is one of the dominant factors controlling the overall electronic properties of a junction, developing efficient methods to fabricate multiple, uniform parallel unimolecular devices is a key target for research and development [13–15].

In order to unify the molecular arrangement within a junction, various studies have been carried out on dense, well-ordered monolayers of the active molecule or on heterogeneous films in which the active molecule is supported within an inert (non-

* Corresponding author.
** Corresponding author.
E-mail addresses: joseluis@unizar.es (J.L. Serrano), smartins@unizar.es (S. Martín).

https://doi.org/10.1016/j.mtchem.2022.101067

conductive) monolayer [8,16–20]. Whilst the electrical properties of these film-based junctions have often proven more reproducible and robust than single-molecule junctions formed from sub-monolayer distributions or from dilute solution [13,21–24], strong coupling effects and other intermolecular interactions can affect the properties of the individual molecules and/or the device [25–27]. In turn, this leads to differences in the electrical properties of single-molecule and thin-film junctions based on the same molecule. Therefore, there is an on-going interest in the development of methods that allow the fabrication of stable, large-area molecular network of unimolecular devices, in which the molecules are placed in defined positions on the surface relative to each other, and at a sufficient distance to avoid potentially deleterious intermolecular coupling effects.

The use of large 'lily-pad' anchor groups to control molecular arrangement and intermolecular distances within multimolecule junctions has met with some success, exemplified by the triazatriangulene platform (TATA) which has been functionalised by various wire-like or switching motifs such as azobenzene derivatives [28–30], porphyrins [31], phenylenes [32], or diarylethenes [33] and assembled into regular patterns over a gold surface. However, such approaches lack a degree of flexibility, with any desired variation in molecular function or structure requiring challenging, pre-assembly synthetic processes. The 'lily-pad' anchor and the functional component also require cooperative design, as the inter-molecule spacing can be influenced by the steric bulk of the functional component if it exceeds the dimensions of the anchor [31].

A more modular approach to the construction of well-defined platform for the parallelisation of single-molecule junctions has been described by Morgado et *al.* [34,35]. A self-assembled monolayer of zinc(II) octaethylporphyrin is used to provide a regular array of zinc binding sites over a HOPG surface. Alternate axial coordination of 4,4′-bipyridine (bpy) to the zinc site and capping with zinc(II) octaethylporphyrin leads to the step-wise construction of conductive structures normal to the surface. Whilst impressively long (ca. 14 nm) self-assembled 1D supramolecular structures were formed by this step-by-step "bottom-up" procedure, surface imaging revealed various defects and incomplete monolayer formation. More recently, a sequential assembly of prototypical iron porphyrins and axial ligands that can be steered via temperature-programmed desorption under ultra-high vacuum conditions has been reported [36]. Although highly effective, the use of ultra-high vacuum conditions and thermal processing steps can limit the applicability of this approach.

With these antecedents in mind, we have developed a versatile, modular layer-by-layer (LbL) strategy for the assembly of well-ordered, parallel arrays of single-molecule structures on gold. In this work, complementary metalloporphyrin and molecular wire moieties are alternately deposited into a densely packed array, simultaneously controlling the stoichiometry of the assembly, and the position (and hence inter-molecule separation) of the molecular wires on the surface. Crucially, in this new approach, the porphyrin moieties in each layer are functionalised by large coumarin-based dendrons. These large pendant groups, which efficiently infill the monolayer and improve the surface coverage, are subsequently photochemically cross-linked to create an ordered film in which wire-like structures are physically well separated from each other and robustly secured to the substrate.

2. Results and discussion

The metallated porphyrin **1** (Scheme 1) was selected for this work, as: i) it forms highly-ordered monolayers on metal surfaces, with the porphyrin core and dendrons lying flat against the surface to maximize dispersion interactions [37–39]; ii) the metallated porphyrin core provides a well-defined "anchor" point to coordinate functional molecules and build the next layer of the growing supramolecular component; and iii) each porphyrin core is surrounded by four dendron units derived from a 3,4,5-trialkoxycarboxylic acid bearing three coumarins, which are linked to the apical aromatic group by means of a flexible undecamethylene spacer to promote their mobility and ensure conformity with the surface.

The dendrons at the periphery of **1** define and occupy the space around the porphyrin core, providing sufficient separation between the neighbouring positions for attachment of functional molecules in a well-ordered array. Cross-linking through photodimerization of the coumarin units locks the positions of the porphyrins in the monolayer [40,41]. The bi-functional molecular wire **2** [42] and closely related ferrocene derivative **3** were selected due to the strong interaction of the amine group with the Zn-metal ion of the porphyrin core (a binding energy of NH_3 to zinc (II) -tetraphenylporphyrin of 49 $kJ \cdot mol^{-1}$ has been determined [43]). Whilst **2** allows layer-by-layer (LbL) assembly of multi-layer structures, **3** serves as redox-active marker through which to evaluate the stoichiometry of the self-assembly process (Scheme 1).

A homogeneous, well-ordered monolayer film of **1** was assembled onto either gold on glass substrates (Arrandee, Germany) flame-annealed at approximately 800–1000 °C with a Bunsen burner flame to obtain atomically flat Au(111) terraces before use [44], or gold on mica substrates (Georg Albert PVD Beschichtunben, Germany, used as received), using the Langmuir-Blodgett (LB) technique (Scheme 1, *step 1*). The use of the LB technique to assemble the base layer of **1** proved key to obtain densely and orderly packed films. By controlling the area per molecule within the initial Langmuir film (Fig. S10) at the air-water interface prior to transfer to the gold substrate the formation of aggregates and columnar stacks could be avoided; these issues plagued the efforts to create good quality monolayers by self-assembly (SA) of **1** from solution (Fig. S11). Quartz crystal microbalance (QCM) measurements allowed us to quantitatively determine the surface coverage of the film from the difference in the resonator frequency (Δf) before and after the LB film formation process using the relationship described by the Sauerbrey equation (Section S4) [45]. The frequency variation of −6 Hz gives a surface coverage of 16.1 $nm^2 \cdot molecule^{-1}$, which compares with the value of ca. 18 $nm^2 \cdot molecule^{-1}$ estimated from the molecular area of **1** (totally extended) lying flat on the substrate (as estimated within the Spartan suite of programs).

The X-ray photoelectron spectrum (XPS) of a powder sample of **1** in the Zn(2*p*) region contains a single peak at 1022.1 eV arising from the characteristic spin–orbit splitting of Zn($2p_{3/2}$) (Fig. S12). In the XPS one N(1*s*) core level peak at 399.4 eV is also observed, as expected for the metalloporphyrin as **1**, with four equivalent nitrogen atoms bonded to zinc [46,47]. In contrast, the XPS of the LB film of **1** on gold displays peaks attributed to the Zn($2p_{3/2}$) and N(1*s*) at lower binding energies (1021.5 and 398.8 eV, respectively, Fig. S12). These data are consistent with the porphyrin moieties lying flat and permitting the Zn and N atoms to interact with the gold electrode surface. The samples showed good stability during the XPS analysis, maintaining the same spectral features and composition throughout the measurement.

The gold-supported LB film of **1** was irradiated at 365 nm for 15 min to promote photodimerization of the coumarin units and lock the film structure by these new cross-links. This process was optimized by observing the decrease in intensity of the characteristic UV–vis spectroscopic features of the coumarin moiety during irradiation. After 15 min no further significant changes were observed. The resulting network, **Au|1** (Scheme 1, *step 2*), avoids

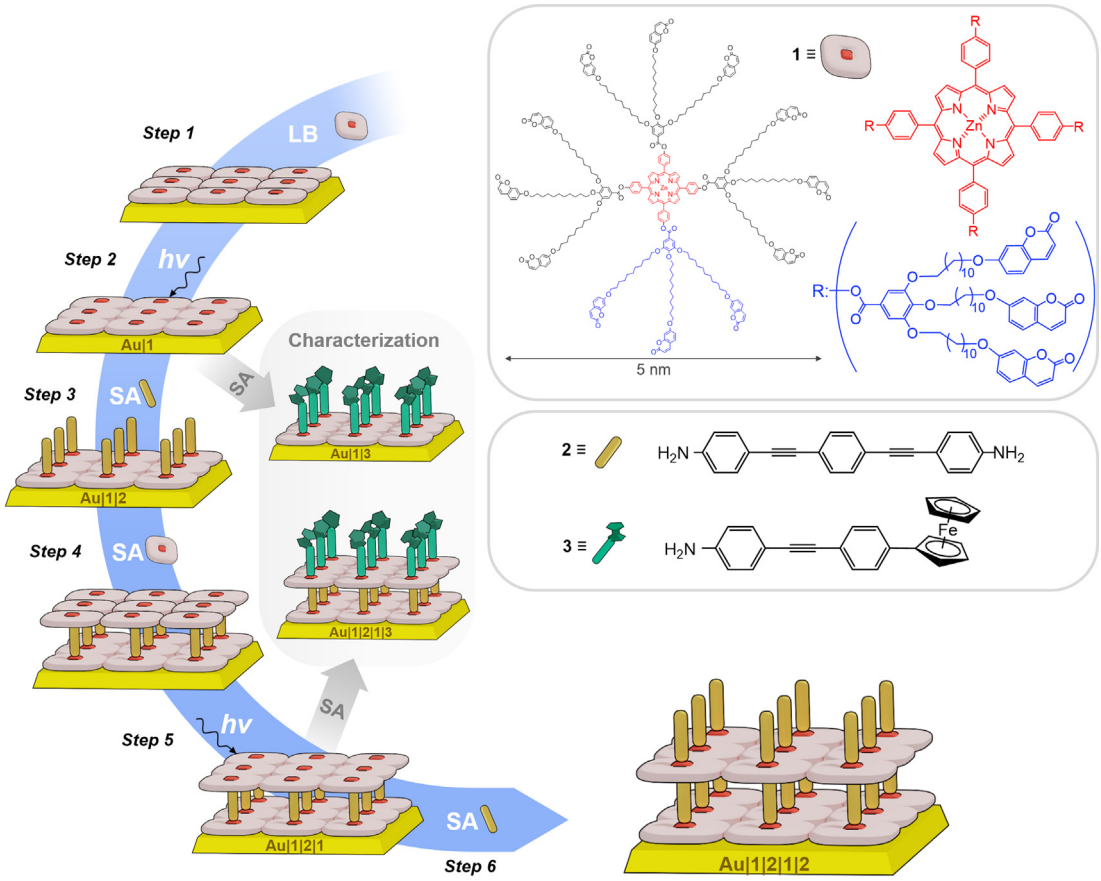

Scheme 1. Structures of the zinc porphyrin-cored dendrimer, **1** (used to fabricate the molecular platform), compound **2** (which serves as the bifunctional molecular wire in the unimolecular scaffolding), and compound **3** (used as a probe of the stoichiometry of the self-assembling layer-by-layer (LbL) process). The LbL strategy for assembling a large-area parallel array of single-supramolecular wires with cross-linked porphyrin scaffolding. (*step 1*: formation of a LB film of **1**; *step 2 and 5*: photodimerization cross-linking of **1**; *step 3 and 6*: self-assembly of **2** or **3**; and *step 4*: self-assembly of **1**).

exposed areas of the gold substrate between neighbouring porphyrin cores, and analysis of the surface by AFM imaging after cross-linking reveals a homogenous film without defects or evidence of columnar stacks (Fig. 1a). The thickness of the cross-linked film of **1** was determined to be only 0.5 ± 0.1 nm by the AFM tip lithography method (Fig. S13), consistent with retention of the flat orientation of **1** on the surface and corroborated by estimates of the film thickness made from attenuation of the Au(4f) signal (Fig. S14). With just the single, flat-lying, cross-linked layer of **1** on the gold surface (**Au|1**) the step and terrace structure of the substrate is clearly visible (Fig. 1a, upper image).

A high resolution STM image of the gold-supported LB film of **1** after cross-linking reveals a regular array of bright points, each corresponding to a porphyrin unit (Fig. 2); irregularities observed in Fig. 2 are attributed to defects on the surface of the underlying gold substrate. Steps on the gold substrate are clearly resolved, alongside the individual porphyrin molecules in the film. The uniformity of the porphyrin arrangement is also clearly shown on the corresponding profile traced across the white line marked on the topography STM image. The 5–8 nm separation of porphyrin units is in excellent agreement with the calculated molecular dimensions of **1** (ca. 5 nm, Scheme 1) and in good agreement with the area per molecule previously determined from QCM measurements. Together, the XPS, AFM and STM data indicate that the Zn anchor points at the centre of the porphyrin moiety of **1** are arranged in a regular fashion on the Au surface after cross-linking, and define a 2D surface bound base layer for building a regio-regular array of unimolecular scaffolding over a large area.

Before assembling extended structures using coordination interactions between the metalloporphyrin **1** and the bifunctional, wire-like OPE derivative **2** outline in Scheme 1, the basic concept was tested using the model, redox-active compound **3**. To confirm the viability of the coordination step, a gold substrate modified by a cross-linked film of **1** was incubated in a 10^{-4} M solution of **3** in ethanol for 24 h (Scheme 1, *step 3*). The axial coordination of **3** to the zinc binding sites on the surface of the modified **Au|1** substrate to give **Au|1|3** structures was verified by both XPS (Fig. 3a) and electrochemical measurements (Fig. 3b). In the XPS, the characteristic Fe($2p_{3/2}$) peak is observed at 707.6 eV, in good agreement with data from a powder sample of **3** (Fig. S17). In the N(1*s*) region a peak at 398.7 eV arises from the four equivalent nitrogen atoms of the porphyrin core [46,47], while the peak at higher binding energy (400.0 eV) is attributed to the N atoms of the amine moieties of **3** which are coordinated to the zinc atoms of the monolayer of **1** template (Fig. 3a) [48,49]. This compares with the equivalent N1s peaks in the powder sample of **3** at 399.4 eV (Fig. S18) and the characteristically shifted signal at 401.2 eV arising from the interaction of a primary arylamine directly with a gold substrate [42].

Cyclic voltammetry (CV) measurements were made using the **Au|1|3** films as a working electrode in a 0.1 M $KClO_4$ electrolyte solution. Within the resulting voltammograms, a single pair of current peaks (P1, P1′) are identified, which are attributed to the

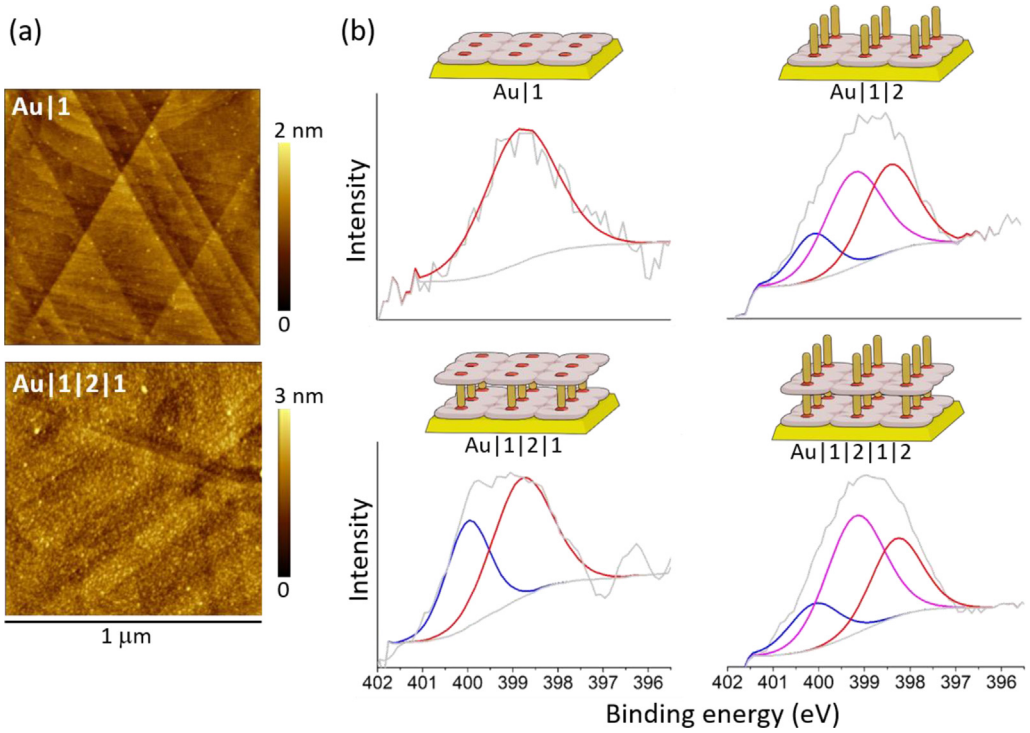

Fig. 1. (a) AFM images of a film of **1** transferred at the area per molecule of 18 nm^2 onto a gold substrate and cross-linked (**Au|1**) and for the LbL **Au|1|2|1** structure with cross-linked top layer. (b) XPS spectra of the N1s region after sequential assembly (and cross-linking in the case of **1**) of multi-layer structures (red: four equivalent porphyrin nitrogen atoms bonded to zinc; pink: free NH_2 of **2**; blue: NH_2 of **2** interacting with the metal porphyrin core). (For interpretation of the references to colour in this figure legend, the reader is referred to the Web version of this article.)

ferrocene (Fc) oxidation and ferrocenium reduction, respectively (Fig. 3b). The anodic and cathodic peak current density J_{pa} and J_{pc} scale linearly with the scan rate, indicating a surface-confined electron transfer (ET) reaction. Meanwhile, the surface concentration of active ferrocene groups attached covalently to the metal porphyrin core, Γ_{Fc}, determined from the electrochemical data (17.2 $nm^2 \cdot molecule^{-1}$) is consistent with the incorporation of **3** in a 1:1 stoichiometric ratio to the molecular platform (Section S9).

With the coordination of **3** to the metalloporphyrin established, the heterogeneous rate constant, k_{ET}, between the ferrocene groups and the gold substrate was calculated using the Laviron analysis ($k_{ET} = 3.4 \pm 0.3\ s^{-1}$, Fig. S20). This electron transfer rate is similar to that determined for electron transfer between a gold substrate electrode and Fc groups covalently attached by click chemistry to an octatetrayne monolayer of comparable thickness to the tolane-like film of **3** ($k_{ET} = 3.2 \pm 0.1\ s^{-1}$) [20]. The electron transfer rate is also similar to that obtained for a ferrocene-terminated peptide nucleic acid (PNA) SAM (k_{ET} ~3 s^{-1}) [50], which is known to exhibit high conductance values [51,52]. These electrochemical results demonstrate reasonably efficient ET between the underlying gold electrode surface and the distal ferrocene groups of **3** through the wire-like tolane (and hence OPE) molecular backbone and cross-linked base-layer of **1**.

Following the successful coordination of **3** to the modified **Au|1** substrate, the same methodology was used to construct well-ordered **Au|1|2** films, by incubating **Au|1** for 24 h in a 10^{-4} M solution of wire-like **2** [42,53] in ethanol (Scheme 1, *step 3*). The XPS data for the N(1*s*) region from this system displays a broad feature that can be deconvoluted into three peaks (Fig. 1b) at: 398.3 eV, assigned to the four equivalent N atoms of the porphyrin moieties

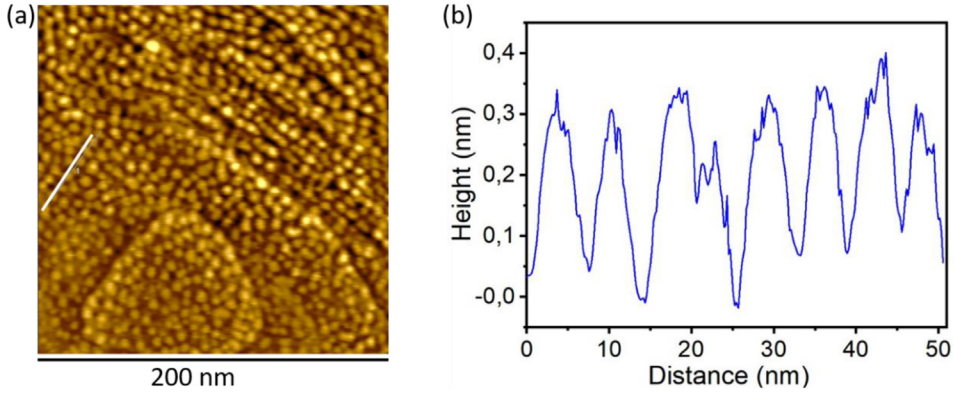

Fig. 2. (a) STM image of a gold-supported LB film of **1** after cross-linking (tunneling current set point, 0.2 nA; voltage bias, −0.6 V, in air at room temperature). The white line represents the trace of the STM tip from which the profile of porphyrin units shown in panel (b) was determined. (For interpretation of the references to colour in this figure legend, the reader is referred to the Web version of this article.)

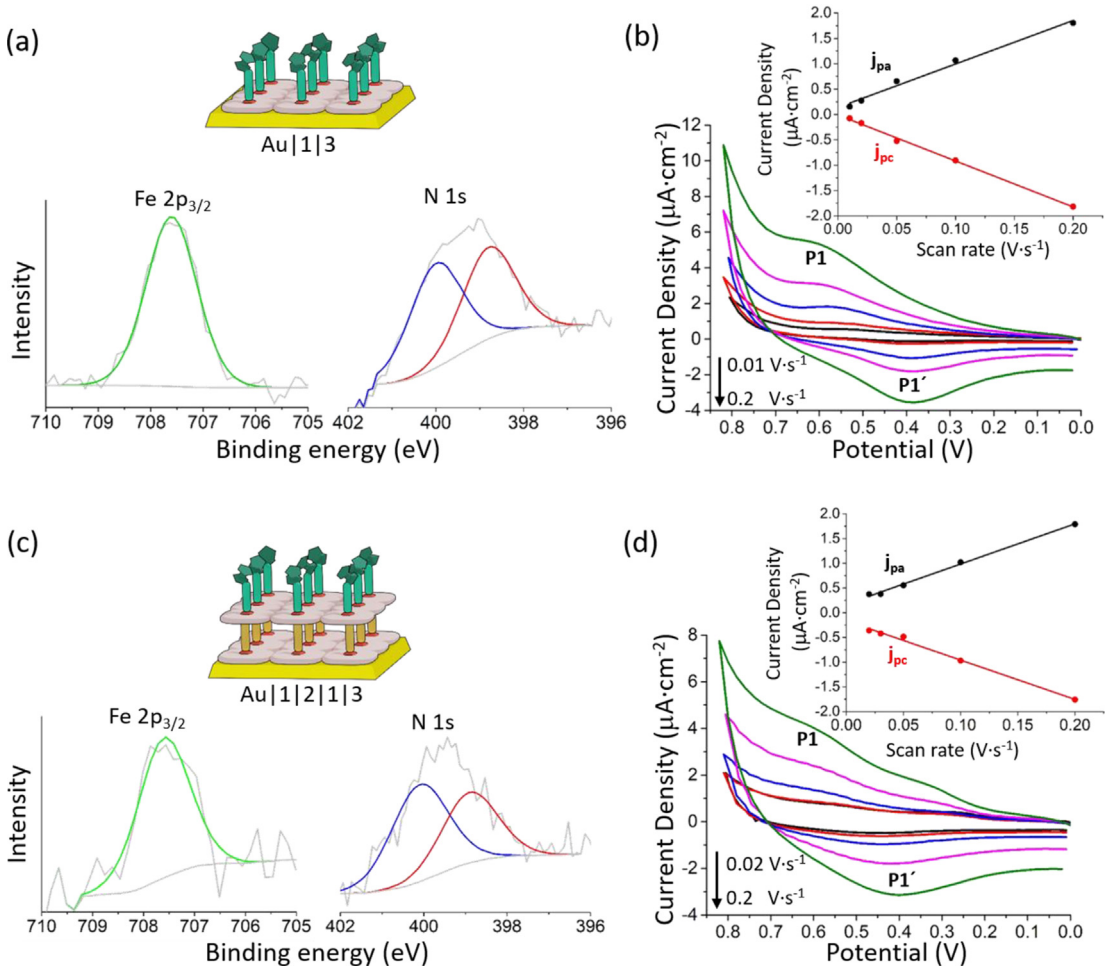

Fig. 3. (a, c) XPS spectra of the Fe2$p_{3/2}$ and N1s region for the **Au|1|3** and **Au|1|2|1|3** structures, respectively (red: four equivalent porphyrin nitrogen atoms bonded to zinc; blue: NH_2 of **3** interacting with the metal porphyrin core), (b, d) Cyclic voltammograms recorded for the indicated structures in a 0.1 M $KClO_4$ electrolyte solution and at the indicated scan rates. Inset: Faradaic cathodic and anodic peak current densities exhibiting a linear dependence with scan rate. (For interpretation of the references to colour in this figure legend, the reader is referred to the Web version of this article.)

in the templating base layer interacting with the gold substrate [46,47]; 400.1 eV due to the N atoms of the amine moieties of **2** coordinated to the zinc centres of the template layer of cross-linked **1** [48,49]; and 399.1 eV which is almost identical to binding energy observed for the powder sample of **2** (Fig. S16) and assigned to the uncoordinated amine functional groups now decorating the top layer of the film (Fig. 1b). In addition, the XPS data for the Zn(2*p*) region for this system shows a slight shift towards lower binding energies (1021.1 eV) with respect to the signal arising from the **Au|1** structure (1021.5 eV), providing further evidence for the coordination of **2** to the base layer of **1** (Fig. S19).

The nanostructured **Au|1|2** film was progressively and sequentially functionalised by a further layer of the Zn porphyrin, which was cross-linked prior to further assembly of **2** or **3** to give multilayer structures (Scheme 1). Initial attempts to construct these multiple layers using LB methods to deposit the second layer of **1** resulted in indiscriminate association of the porphyrin to the **Au|1|2** surface following the physical transfer of the Langmuir layer and cross-linking to give a multi-layer structure, **Au|1|2|1***. The newly deposited, but mismatched layer (denoted **1***), contacts to the underlying film through van der Waals interactions, rather than more selective interactions by coordination of the zinc ion to the free amine moieties of **2** decorating the film surface. The lack of registry between the base **Au|1|2** film and the new layer of **1*** resulted in poor electron transfer characteristics when the mismatched assembly **Au|1|2|1*** was further functionalised by **3** (Section S11).

To create a more ordered multilayer structure with better registry between the layers, a film of the zinc porphyrin **1** was self-assembled onto the **Au|1|2** base structures. A very dilute solution of **1** was used for this self-assembly step (10^{-6} M) to prevent aggregation and columnar stacking, as well as to promote coordination of zinc ion in the metal porphyrin core to the free amine of **2** (Scheme 1, *step 4*). The new porphyrin layer was photochemically cross-linked (Scheme 1, *step 5*) and the resulting **Au|1|2|1** structure characterised by a combination of QCM, AFM imaging and XPS data (Fig. 1, Fig. S15, Fig. S23), revealing that this subsequent layer maintains the same surface coverage and uniform surface structure as the base **Au|1** structure. The thickness of this multilayer structure **Au|1|2|1** (1.6 ± 0.1 nm) with a cross-linked top-layer was obtained by atomic force microscopy (AFM) lithography (pit-etching or scratching) in excellent agreement with the molecular dimensions of the components (Fig. S15). The terraces and surface features of the substrate are less apparent in AFM images of this thicker layer (Fig. 1b) than in images of the initial template layer **Au|1** (Fig 1a). Given the surface coverage of the template, the stoichiometry and registry of the multi-layer assembly with the zinc porphyrin sites from which these structures grow, it can be estimated that within the **Au|1|2|1** film, 6.2×10^{12} molecules·cm^{-2} are

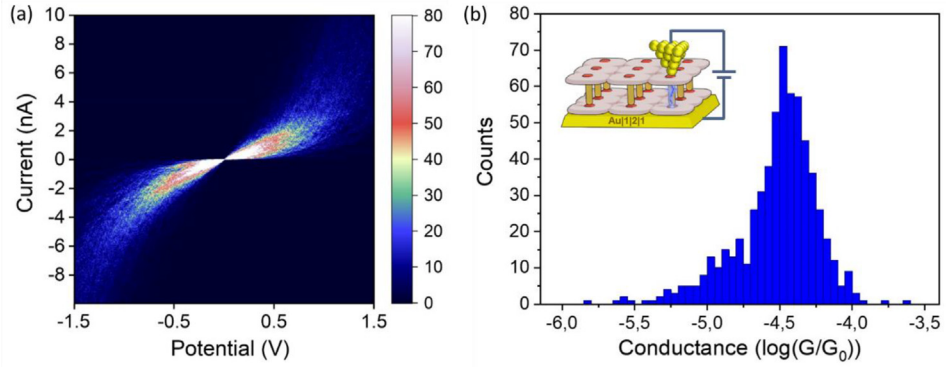

Fig. 4. (a) *I*–*V* curves experimentally obtained (ca. 600) by positioning the STM tip on top of the **Au|1|2|1** structure. (b) Conductance histogram built by adding all the experimental data from −0.5 to +0.5 V for each *I*–*V* curve obtained. Inset: Cartoon showing the determination of the electrical properties of the **Au|1|2|1** structure by using the "STM touch-to-contact" method.

arranged in a parallel fashion. Each of these corresponds to a unimolecular device, some 1.6 nm in height (Fig. S15) and separated from each other by 5–8 nm (Fig. 2) positioned across the substrate surface.

The LbL assembly of wire-like moieties of **2** on a template base-layer of **1** represents a strategy to fabricate multiple, uniform parallel unimolecular devices with the molecules in defined positions and sufficiently well-separated (ca. 5 nm) to avoid intermolecular coupling effects (Scheme 1). To demonstrate this capacity, the new **Au|1|2|1** multilayer structure was capped or extended through further reactions with **3** or **2**, respectively (Scheme 1, *step 6*). The resulting **Au|1|2|1|3** and **Au|1|2|1|2** films were also characterised by CV and XPS data (Fig. 3, Fig. S20) and by XPS (Fig. 1, Fig. S23), respectively, with each subsequent layer maintaining the same surface coverage and uniform surface structure as the underlying **Au|1|2|1** structure. Whilst the mismatched **Au|1|2|1*****|3** structure proved to effectively block electron transfer between the ferrocene redox marker and the gold substrate (Section S11), the self-assembled **Au|1|2|1|3** gave a value of k_{ET} = 4.1 ± 0.6 s^{-1} (Fig. S20), which indicates efficient ET between the ferrocene head group and the Au substrate through the well-ordered and extended wire-like |**1**|**2**|**1**| assembly.

The electrical properties of the **Au|1|2|1** structure were determined using the STM "touch-to-contact" method (a variation of the STM current–distance (*I*(*s*)) method [54]), which is particularly well-suited for the formation of single-molecule junctions from monolayer films [18,55]. In brief, following determination of film thickness by an independent method and calibration of the tip-substrate separation, a STM tip (which is electrochemically etched to be atomically sharp) is positioned just above the top surface of a molecular monolayer. This allows a substrate|molecule|STM tip junction to form, the electrical properties of which can then be determined upon application of a suitable bias in a manner entirely analogous to the many other STM-based molecular junction methods developed in recent years [56,57].

Effective use of the STM "touch-to-contact" method requires determination of the tip to substrate distance at which the STM tip touches the top of the film. Calibration of the tip–substrate distance (*s*) was achieved by calculating the absolute gap separation (*s*) from the set-point parameters (set-point current, I_0, and tip bias, U_t) (Section S13). With $d\ln I/ds = 6.3 \pm 1.6\ nm^{-1}$ and set-point parameters of $I_0 = 2$ nA and $U_t = 0.6$ V, the tip–substrate distance is estimated to be 1.6 nm (Section S13, equation 4). Therefore, using these set-point parameters, current–voltage (*I*–*V*) curves can be recorded with the tip just in contact with the top of the **Au|1|2|1** structure. Fig. 4a shows the *I*–*V* curves (ca. 600) recorded from different locations and various substrates using these touch-to-contact conditions. The *I*–*V* data exhibits characteristic sigmoidal shape over the bias window from −1.5 V to +1.5 V and are symmetrical around zero bias (i.e. no current rectification). From the low-voltage region (from −0.5 to +0.5 V), which shows approximately linear ohmic behaviour, a conductance value can be determined for each curve. A conductance histogram built from these conductance values from all 600 *I*–*V* curves gives a most probable molecular conductance of $10^{-4.4}$ G_0 (Fig. 4b). This value is consistent with values for single molecule conductance of **2** determined using the STM break junction method or the *I*(*s*) technique ($10^{-4.6}$–$10^{-3.9}$ G_0) [42,58]. This finding highlights that single molecule electrical behaviour is retained within the film, and that the cross-linked porphyrin film onto which the OPE wire-like molecule **2** is assembled has no significant effect on the single molecule conductance.

3. Conclusions

In summary, a new layer-by-layer (LbL) strategy for the reproducible self-assembly of multi-layer devices with excellent spatial control over large substrate area has been developed. Bulky dendrons on the periphery of a zinc metalloporphyrin are used to spatially order these nascent metal ion building sites regioregularly across a gold electrode surface, before being cross-linked to stabilise the film structure. The molecular devices are synthesized on surface by taking advantage of the facile coordination of an α,ω-amino functionalised oligo(phenylene)ethynylene (OPE) molecule to the zinc ions of the metalloporphyrin template base-layer. The structure is then extended through a second, self-assembled zinc porphyrin layer which is cross-linked before being further extended by coordination with a second layer of the OPE. The coordination interaction between the zinc(II) sites and the bifunctional OPE wire ensures a high degree of registry between the layers and good electrical contact through the extended arrays and offers fine control over the chemical composition. In this manner, the regular arrangement of isolated molecules over a substrate with dimensions controlled by the supporting dendrons is achieved, with the separation of the constituent molecules suppressing cross-talk and in-plane charge transport within the layer. Furthermore, in principle, this on surface, layer-by-layer self-assembly strategy allows the structure of the functional molecule to be readily adapted to suit the desired application. Consequently, future work will be devoted to assessing the suitability of this platform with molecular components exhibiting a wider range of electrical function, and exploiting the free volume between active molecules to allow facile, shape dependent molecular effects, with devices such as electromechanically operated switches being targeted.

CRediT authorship contribution statement

Enrique Escorihuela: Data curation, Investigation, Methodology, Software, Visualization, Validation. **Alberto Concellón**, **Iván Marín**, **Varshini J. Kumar**, **Lucía Herrer and Stephen A. Moggach**: Resources. **Andrea Vezzoli and Richard J. Nichols**: Formal Analysis, Software, Funding acquisition. **Paul J. Low**: Resources, Funding acquisition, Writing - Review & Editing. **Pilar Cea**: Conceptualization, Funding acquisition, Writing - Review & Editing. **José Luis Serrano**: Conceptualization, Funding acquisition, Writing - Review & Editing. **Santiago Martín**: Investigation, Methodology, Visualization, Writing - Review & Editing. All authors writing-review & editing.

Declaration of competing interest

The authors declare that they have no known competing financial interests or personal relationships that could have appeared to influence the work reported in this paper.

Acknowledgements

E.E. gratefully acknowledges the award of a DGA fellowship from the Government of Aragon and Campus Iberus – Erasmus+Programme, Universidad de Zaragoza, Fundación Bancaria Ibercaja, and Fundación CAI (CB 7/21) for extranational research stays co-funding. P.C., J.L.S. and S.M. are grateful for financial assistance in the framework of the projects PID2019-105881RB-I00 funded by MCIN/AEI/10.13039/501100011033 and PGC-2018-097583-I00 and Gobierno de Aragón through the grants E31_20R and E47_20R with European Social Fund (Construyendo Europa desde Aragón). P.J.L. thanks the Australian Research Council for generous funding through DP190100073 and DP190100074. V.J.K. gratefully acknowledges scholarship and support from the Schlumberger Foundation through the Faculty for the Future Program and the Scholarship for International Research Fees from the University of Western Australia. S.A.M. holds an ARC Future Fellowship (FT200100243). AV thanks the Royal Society for generous funding (Fellowship URFøR1ø191241). RJN thanks EPSRC for funding (EP/M029522/1 and EP/M014169/1) and funding from the Leverhulme Foundation (RPG-2019-308).

Appendix A. Supplementary data

Supplementary data to this article can be found online at https://doi.org/10.1016/j.mtchem.2022.101067.

References

[1] S.C. Zhang, H. Liu, J.Y. Yu, B.Y. Li, B. Ding, Multi-functional flexible 2D carbon nanostructured networks, Nat. Commun. 11 (2020) 5134.
[2] P.J. Santos, P.A. Gabrys, L.Z. Zornberg, M.S. Lee, R.J. Macfarlane, Macroscopic materials assembled from nanoparticle superlattices, Nature 591 (2021) 586–591.
[3] C.P. Xu, A.R. Puente-Santiago, D. Rodriguez-Padron, M.J. Munoz-Batista, M.A. Ahsan, J.C. Noveron, R. Luque, Nature-inspired hierarchical materials for sensing and energy storage applications, Chem. Soc. Rev. 50 (2021) 4856–4871.
[4] T.A. Su, M. Neupane, M.L. Steigerwald, L. Venkataraman, C. Nuckolls, Chemical principles of single-molecule electronics, Nat. Rev. Mater. 1 (2016) 16002.
[5] T. Li, W.P. Hu, D.B. Zhu, Nanogap electrodes, Adv. Mater. 22 (2010) 286–300.
[6] L. Sun, Y.A. Diaz-Fernandez, T.A. Gschneidtner, F. Westerlund, S. Lara-Avila, K. Moth-Poulsen, Single-molecule electronics: from chemical design to functional devices, Chem. Soc. Rev. 43 (2014) 7378–7411.
[7] D. Xiang, X.L. Wang, C.C. Jia, T. Lee, X.F. Guo, Molecular-scale electronics: from concept to function, Chem. Rev. 116 (2016) 4318–4440.
[8] H. Jeong, D. Kim, D. Xiang, T. Lee, High-yield functional molecular electronic devices, ACS Nano 11 (2017) 6511–6548.
[9] J.Y. Liu, X.Y. Huang, F. Wang, W.J. Hong, Quantum interference effects in charge transport through single-molecule junctions: detection, manipulation, and application, Acc. Chem. Res. 52 (2019) 151–160.
[10] C.W. Fuller, P.S. Padayatti, H. Abderrahim, L. Adamiak, N. Alagar, N. Ananthapadmanabhan, J. Baek, S. Chinni, C. Choi, K.J. Delaney, R. Dubielzig, J. Frkanec, C. Garcia, C. Gardner, D. Gebhardt, T. Geiser, Z. Gutierrez, D.A. Hall, A.P. Hodges, G. Hou, S. Jain, T. Jones, R. Lobaton, Z. Majzik, A. Marte, P. Mohan, P. Mola II, P. Mudondo, J. Mullinix, T. Nguyen, F. Ollinger, S. Orr, V. Ouyang, P. Pan, N. Park, D. Porras, K. Prabhu, C. Reese, T. Ruel, T. Sauerbrey, J.R. Sawyer, P. Sinha, J. Tu, A.G. Venkatesh, S. VijayKumar, L. Zheng, S. Jin, J.M. Tour, G.M. Church, P.W. Mola, B. Merriman, Molecular electronics sensors on a scalable semiconductor chip: a platform for single-molecule measurement of binding kinetics and enzyme activity, Proc. Natl. Acad. Sci. USA 119 (2022), 2112812119.
[11] H.M. Liu, N. Wang, J.W. Zhao, Y. Guo, X. Yin, F.Y.C. Boey, H. Zhang, Length-dependent conductance of molecular wires and contact resistance in metal-molecule-metal junctions, ChemPhysChem 9 (2008) 1416–1424.
[12] W. Haiss, S. Martin, E. Leary, H. van Zalinge, S.J. Higgins, L. Bouffier, R.J. Nichols, Impact of junction formation method and surface roughness on single molecule conductance, J. Phys. Chem. C 113 (2009) 5823–5833.
[13] A. Vilan, D. Aswal, D. Cahen, Large-area, ensemble molecular electronics: motivation and challenges, Chem. Rev. 117 (2017) 4248–4286.
[14] A. Nitzan, M.A. Ratner, Electron transport in molecular wire junctions, Science 300 (2003) 1384–1389.
[15] T.A. Gschneidtner, Y.A.D. Fernandez, K. Moth-Poulsen, Progress in self-assembled single-molecule electronic devices, J. Mater. Chem. C 1 (2013) 7127–7133.
[16] S. Casalini, C.A. Bortolotti, F. Leonardi, F. Biscarini, Self-assembled monolayers in organic electronics, Chem. Soc. Rev. 46 (2017) 40–71.
[17] L. Herrer, S. Martin, A. Gonzalez-Orive, D.C. Milan, A. Vezzoli, R.J. Nichols, J.L. Serrano, P. Cea, pH control of conductance in a pyrazolyl Langmuir-Blodgett monolayer, J. Mater. Chem. C 9 (2021) 2882–2889.
[18] E. Escorihuela, P. Cea, S. Bock, D.C. Milan, S. Naghibi, H.M. Osorio, R.J. Nichols, P.J. Low, S. Martin, Towards the design of effective multipodal contacts for use in the construction of Langmuir-Blodgett films and molecular junctions, J. Mater. Chem. C 8 (2020) 672–682.
[19] L. Herrer, A. Ismael, S. Martin, D.C. Milan, J.L. Serrano, R.J. Nichols, C. Lambert, P. Cea, Single molecule vs. large area design of molecular electronic devices incorporating an efficient 2-aminepyridine double anchoring group, Nanoscale 11 (2019) 15871–15880.
[20] A. Moneo, A. Gonzalez-Orive, S. Bock, M. Fenero, I.L. Herrer, D.C. Milan, M. Lorenzoni, R.J. Nichols, P. Cea, F. Perez-Murano, P.J. Low, S. Martin, Towards molecular electronic devices based on 'all-carbon' wires, Nanoscale 10 (2018) 14128–14138.
[21] D. Vuillaume, Molecular electronics: from single-molecule to large-area devices, ChemPlusChem 84 (2019) 1215–1221.
[22] H.B. Akkerman, P.W.M. Blom, D.M. de Leeuw, B. de Boer, Towards molecular electronics with large-area molecular junctions, Nature 441 (2006) 69–72.
[23] E. Gorenskaia, K.L. Turner, S. Martin, P. Cea, P.J. Low, Fabrication of metallic and non-metallic top electrodes for large-area molecular junctions, Nanoscale 13 (2021) 9055–9074.
[24] L. Herrer, S. Martin, P. Cea, Nanofabrication techniques in large-area molecular electronic devices, Appl. Sci. 10 (2020) 6064.
[25] H. Song, H. Lee, T. Lee, Intermolecular chain-to-chain tunneling in metal-alkanethiol-metal junctions, J. Am. Chem. Soc. 129 (2007) 3806–3807.
[26] Y. Dubi, Transport through self-assembled monolayer molecular junctions: role of in-plane dephasing, J. Phys. Chem. C 118 (2014) 21119–21127.
[27] K. Slowinski, R.V. Chamberlain, C.J. Miller, M. Majda, Through-bond and chain-to-chain coupling. Two pathways in electron tunneling through liquid alkanethiol monolayers on mercury electrodes, J. Am. Chem. Soc. 119 (1997) 11910–11919.
[28] H. Jacob, S. Ulrich, U. Jung, S. Lemke, T. Rusch, C. Schutt, F. Petersen, T. Strunskus, O. Magnussen, R. Herges, F. Tuczek, Monitoring the reversible photoisomerization of an azobenzene-functionalized molecular triazatriangulene platform on Au(111) by IRRAS, Phys. Chem. Chem. Phys. 16 (2014) 22643–22650.
[29] U. Jung, S. Kuhn, U. Cornelissen, F. Tuczek, T. Strunskus, V. Zaporojtchenko, J. Kubitschke, R. Herges, O. Magnussen, Azobenzene-containing triazatriangulenium adlayers on Au(111): structural and spectroscopic characterization, Langmuir 27 (2011) 5899–5908.
[30] S. Kuhn, B. Baisch, U. Jung, T. Johannsen, J. Kubitschke, R. Herges, O. Magnussen, Self-assembly of triazatriangulenium-based functional adlayers on Au(111) surfaces, Phys. Chem. Chem. Phys. 12 (2010) 4481–4487.
[31] F.L. Otte, S. Lemke, C. Schutt, N.R. Krekiehn, U. Jung, O.M. Magnussen, R. Herges, Ordered monolayers of free-standing porphyrins on gold, J. Am. Chem. Soc. 136 (2014) 11248–11251.
[32] Z.M. Wei, X.T. Wang, A. Borges, M. Santella, T. Li, J.K. Sorensen, M. Vanin, W.P. Hu, Y.Q. Liu, J. Ulstrup, G.C. Solomon, Q.J. Chi, T. Bjornholm, K. Norgaard, B.W. Laursen, Triazatriangulene as binding group for molecular electronics, Langmuir 30 (2014) 14868–14876.
[33] Q. Wang, L. Ma, Z.H. Liu, X. Zhang, Z.Y. Zhang, Z.C. Shangguan, X.H. Huang, Y.Q. Liu, J.T. Lv, H.M. Zhang, L.F. Chi, T. Li, Triazatriangulene platform for self-assembled monolayers of free-standing diarylethene, Sci. China Mater. 61 (2018) 1345–1350.

[34] Q. Ferreira, L. Alcacer, J. Morgado, Stepwise preparation and characterization of molecular wires made of zinc octaethylporphyrin complexes bridged by 4,4 '-bipyridine on Hopg, Nanotechnology 22 (2011), 435604.
[35] Q. Ferreira, A.M. Braganca, L. Alcacer, J. Morgado, Conductance of well-defined porphyrin self-assembled molecular wires up to 14 nm in length, J. Phys. Chem. C 118 (2014) 7229–7234.
[36] Z.S. Wang, K. Qian, M.A. Oner, P.S. Deimel, Y. Wang, S. Zhang, X.X. Zhang, V. Gupta, J. Li, H.J. Gao, D.A. Duncan, J.V. Barth, X. Lin, F. Allegretti, S.X. Du, C.A. Palma, Layer-by-layer epitaxy of porphyrin-ligand Fe(II)-Fe(III) nano-architectures for advanced metal-organic framework growth, ACS Appl. Nano Mater. 3 (2020) 11752–11759.
[37] J. Otsuki, STM studies on porphyrins, Coord. Chem. Rev. 254 (2010) 2311–2341.
[38] X. Ge, C. Manzano, R. Berndt, L.T. Anger, F. Kohler, R. Herges, Controlled formation of an axially bonded co-phthalocyanine dimer, J. Am. Chem. Soc. 131 (2009) 6096–6098.
[39] F. Matino, G. Schull, U. Jana, F. Kohler, R. Berndt, R. Herges, Single azopyridine-substituted porphyrin molecules for configurational and electronic switching, Chem. Commun. 46 (2010) 6780–6782.
[40] A. Concellon, T. Liang, A.P.H.J. Schenning, J.L. Serrano, P. Romero, M. Marcos, Proton-conductive materials formed by coumarin photocrosslinked ionic liquid crystal dendrimers, J. Mater. Chem. C 6 (2018) 1000–1007.
[41] A. Concellon, A.P.H.J. Schenning, P. Romero, M. Marcos, J.L. Serrano, Size-selective adsorption in nanoporous polymers from coumarin photo-cross-linked columnar liquid crystals, Macromolecules 51 (2018) 2349–2358.
[42] Q. Lu, K. Liu, H.M. Zhang, Z.B. Du, X.H. Wang, F.S. Wang, From tunneling to hopping: a comprehensive investigation of charge transport mechanism in molecular junctions based on oligo(p-phenylene ethynylene)s, ACS Nano 3 (2009) 3861–3868.
[43] W. Hieringer, K. Flechtner, A. Kretschmann, K. Seufert, W. Auwarter, J.V. Barth, A. Gorling, H.P. Steinruck, J.M. Gottfried, The surface trans effect: influence of axial ligands on the surface chemical bonds of adsorbed metalloporphyrins, J. Am. Chem. Soc. 133 (2011) 6206–6222.
[44] W. Haiss, D. Lackey, J.K. Sass, K.H. Besocke, Atomic resolution scanning tunneling microscopy images of Au(111) surfaces in air and polar organic-solvents, J. Chem. Phys. 95 (1991) 2193–2196.
[45] G. Sauerbrey, Verwendung von schwingquarzen zur wagung dunner schichten und zur mikrowagung, Z. Phys. 155 (1959) 206–222.
[46] G. Polzonetti, A. Ferri, M.V. Russo, G. Iucci, S. Licoccia, R. Paolesse, Platinum complex/Zn-porphyrin macrosystem assemblies: electronic structure and conformational investigation by x-ray photoelectron spectroscopy, J. Vac. Sci. Technol. A 17 (1999) 832–839.
[47] D.K. Lavallee, J. Brace, N. Winograd, X-ray photoelectron-spectra of N-methyltetraphenylporphyrins – evidence for a correlation of binding-energies with metal-nitrogen bond distances, Inorg. Chem. 18 (1979) 1776–1780.
[48] D.M. Sarno, B.W. Jiang, D. Grosfeld, J.O. Afriyie, L.J. Matienzo, W.E. Jones, Self-assembled molecular architectures on surfaces: new strategies involving metal-organic copolymers, Langmuir 16 (2000) 6191–6199.
[49] D.M. Sarno, L.J. Matienzo, W.E. Jones, X-ray photoelectron spectroscopy as a probe of intermolecular interactions in porphyrin polymer thin films, Inorg. Chem. 40 (2001) 6308–6315.
[50] A. Paul, R.M. Watson, P. Lund, Y.J. Xing, K. Burke, Y.F. He, E. Borguet, C. Achim, D.H. Waldeck, Charge transfer through single-stranded peptide nucleic acid composed of thymine Nucleotides, J. Phys. Chem. C 112 (2008) 7233–7240.
[51] R. Venkatramani, K.L. Davis, E. Wierzbinski, S. Bezer, A. Balaeff, S. Keinan, A. Paul, L. Kocsis, D.N. Beratan, C. Achim, D.H. Waldeck, Evidence for a near-resonant charge transfer mechanism for double-stranded peptide nucleic acid, J. Am. Chem. Soc. 133 (2011) 62–72.
[52] E. Wierzbinski, R. Venkatramani, K.L. Davis, S. Bezer, J. Kong, Y.J. Xing, E. Borguet, C. Achim, D.N. Beratan, D.H. Waldeck, The single-molecule conductance and electrochemical electron-transfer rate are related by a power law, ACS Nano 7 (2013) 5391–5401.
[53] L. Herrer, V. Sebastian, S. Martin, A. Gonzalez-Orive, F. Perez-Murano, P.J. Low, J.L. Serrano, J. Santamaria, P. Cea, High surface coverage of a self-assembled monolayer by in situ synthesis of palladium nanodeposits, Nanoscale 9 (2017) 13281–13290.
[54] W. Haiss, H. van Zalinge, S.J. Higgins, D. Bethell, H. Hobenreich, D.J. Schiffrin, R.J. Nichols, Redox state dependence of single molecule conductivity, J. Am. Chem. Soc. 125 (2003) 15294–15295.
[55] L.M. Ballesteros, S. Martin, S. Marques-Gonzalez, M.C. Lopez, S.J. Higgins, R.J. Nichols, P.J. Low, P. Cea, Single gold atom containing oligo(phenylene) ethynylene: assembly into LB films and electrical characterization, J. Phys. Chem. C 119 (2015) 784–793.
[56] B.Q. Xu, N.J.J. Tao, Measurement of single-molecule resistance by repeated formation of molecular junctions, Science 301 (2003) 1221–1223.
[57] R.J. Nichols, W. Haiss, S.J. Higgins, E. Leary, S. Martin, D. Bethell, The experimental determination of the conductance of single molecules, Phys. Chem. Chem. Phys. 12 (2010) 2801–2815.
[58] R.R. Ferradas, S. Marques-Gonzalez, H.M. Osorio, J. Ferrer, P. Cea, D.C. Milan, A. Vezzoli, S.J. Higgins, R.J. Nichols, P.J. Low, V.M. Garcia-Suarez, S. Martin, Low variability of single-molecule conductance assisted by bulky metal-molecule contacts, RSC Adv. 6 (2016) 75111–75121.